

# Theory of the different photoemission spectra of metallic and insulating $C_{60}$ compounds

Samuel Wehrli,<sup>1,\*</sup> T.M. Rice,<sup>1</sup> and Manfred Sigrist<sup>1</sup>

<sup>1</sup>*Theoretische Physik, ETH-Hönggerberg, CH-8093 Zürich, Switzerland*

(Dated: November 20, 2018)

Metallic  $K_3C_{60}$  shows pronounced structure and a sharp Fermi edge in integrated photoemission spectra (PES) while the insulating  $K_4C_{60}$  and  $K_6C_{60}$  phases display only a broad structureless peak. We find that both types of spectra can be explained by the coupling to the optic vibrations of the  $K^+/C_{60}^{n-}$  ionic lattice. This is suppressed in  $K_3C_{60}$  due to metallic screening but is strong in the insulating phases. We use the non-crossing approximation to calculate the density of states (DOS) of electrons in  $K_3C_{60}$  coupled to the intramolecular  $H_g$  modes in good agreement with the experiment. For  $K_4C_{60}$  and  $K_6C_{60}$  strong coupling to the low energy optic  $K^+/C_{60}^{n-}$  modes controls the DOS and yields broad peaks in the PES. A moment expansion is used to calculate the position and width of these peaks which agree well with the experiment.

PACS numbers: 63.20.Kr, 73.61.Wp, 79.60.Fr

Alkali-metal-doped  $C_{60}$  has been investigated extensively by photoemission spectroscopy (PES) in bulk systems (Ref. 1, 2, 3 and references therein). Recently, Yang et al. measured the electronic band dispersion of  $K_3C_{60}$  in a monolayer system on Ag(111) by angle resolved PES (ARPES) [4]. By comparing angle integrated spectra (AIPES) from several experiments a generic feature emerges which is the striking difference between the spectra of metallic  $K_3C_{60}$  and the insulating  $K_4C_{60}$  and  $K_6C_{60}$  (the former is a Jahn-Teller distorted insulator, the latter a band insulator):  $K_3C_{60}$  shows a metallic spectra with a sharp Fermi edge and distinct structures whereas the insulating phases display a broad Gaussian-peak. In the present work we address this difference. The key ingredient is the large change in coupling strength of the low-energy ( $\omega \approx 10$  meV) optic vibrations of the  $K^+$  ions. These modes cause a net shift of the  $C_{60}$  molecular levels and their interaction is efficiently screened in metallic  $K_3C_{60}$  where it is reduced by a factor  $10^{-4} - 10^{-2}$  [5, 6]. However, in the insulating phases, where metallic screening is absent, they couple strongly ( $g \approx 70$  meV, see below) due to the direct Coulomb interaction of the ionic charge with the photoemission hole. The resulting physics is best illustrated by the toy-model  $H = \omega a^\dagger a + g c^\dagger c (a^\dagger + a)$  where a single electron is coupled to a harmonic oscillator. The corresponding photoemission spectrum is a Poisson distribution  $P(\epsilon) = \sum_n \nu^n e^{-\nu} / n! \delta(\epsilon + [n - \nu]\omega)$  where  $\nu = (g/\omega)^2$  is the average number of excited phonons emitted during the photoemission process. In the insulating phases  $\nu$  is very large ( $\nu \approx 50$ ) and as a result the spectrum becomes incoherent resulting in a Gaussian-like shape. In the following we treat the metallic and insulating phases separately. First, using the non-crossing approximation (NCA), it is shown that the spectrum of metallic  $K_3C_{60}$  is dominated by the coupling to the intramolecular  $C_{60}$  modes. Second, we use moment expansion to calculate position and width of the Gaussian-like spectra of  $K_4C_{60}$

and  $K_6C_{60}$ .

The only modes that couple strongly ( $\lambda \approx 1$ ) in  $K_3C_{60}$  are the intramolecular  $H_g$  modes which cause a splitting of the threefold degenerate LUMO's of  $C_{60}$  (See Ref. 7 for more details). We treat these modes by NCA [8] and neglect the on-site Coulomb interaction ( $U \approx 1$  eV in bulk). This is justified in a monolayer adsorbed on Ag(111) where  $U$  is reduced by the proximity of the metal [9]. Here we restrict our attention to such systems. A similar calculation was performed by Liechtenstein et al. who showed that the width of the plasmon in  $K_3C_{60}$  can be explained by electron-phonon coupling [10]. The Hamiltonian which describes the conduction band of  $K_3C_{60}$  coupled to the  $H_g$  modes is (setting  $\hbar = 1$ )

$$H_{H_g - \text{vib}} = \sum_{j\delta nm} t_{nm}(\delta) c_{j+\delta m}^\dagger c_{jn} + \sum_{j\nu k} \omega_\nu a_{j\nu k}^\dagger a_{j\nu k} + \sum_{jnm} g_\nu c_{jm}^\dagger c_{jn} \left[ C_{nm}^k a_{j\nu k}^\dagger + C_{mn}^k a_{j\nu k} \right]. \quad (1)$$

The first term is the tight-binding band in standard notation formed by the 3-fold degenerate ( $t_{1u}$ ) LUMO's of  $C_{60}$ . The sum is over the orbitals  $n$  and  $m$ , the lattice sites  $j$  and the nearest neighbors  $\delta$ . As the spin orientation is preserved in the Hamiltonian, explicit sums over spins are dropped throughout. The second term is the energy  $\omega_\nu$  of the eight five-fold degenerate  $H_g$  vibrational multiplets [7]. The indices  $\nu$  and  $k$  denote the multiplet and the mode respectively. The last term describes the electron-phonon coupling. The phonon energies  $\omega_\nu$  and the coupling parameters  $g_\nu$  are dispersionless. The parameters  $g_\nu$  are related to the partial coupling constant  $\lambda_\nu$  by  $g_\nu^2 = \frac{3}{2} \omega_\nu \lambda_\nu / N(0)$  where  $N(0)$  is the density of states per spin and molecule [11]. Values for  $\omega_\nu$  and  $\lambda_\nu$  were taken from Ref. 12. The structure of the coupling is given by the coefficients  $C_{nm}^k = \sqrt{\frac{3}{5}} (-1)^m \langle 2, k | 1, -m; 1, n \rangle$  where  $\langle \dots \rangle$  is the Clebsch-Gordan coefficient [13]. The normalization is

such that  $\sum_{knm} (C_{nm}^k)^2 = 3$ . In the NCA, the electron self-energy is determined self-consistently by the lowest order self-energy diagram with the interacting Green's function. In the present problem the Green's function  $G_{nm}(\omega, \mathbf{k})$  and self-energy  $\Sigma_{nm}(\omega, \mathbf{k})$  are  $3 \times 3$  matrices. The free phonon propagator  $D_{\nu k}^0(\omega, \mathbf{q}) = D_{\nu}^0(\omega)$  depends only on frequency and the multiplet. As a consequence, only the local part of the Green's function  $G_{nm}^{\text{loc}} = 1/N \sum_{\mathbf{k}} G_{nm}(\omega, \mathbf{k})$  enters which renders the self-energy  $\Sigma_{nm}(\omega, \mathbf{k}) = \Sigma_{nm}(\omega)$  local as well. This is a consequence of including only non-crossing diagrams. The evaluation of the basic diagram can be simplified further when the symmetry of the lattice is used. The momentum-independent Green's function  $G_{nm}^{\text{loc}}$  and self-energy  $\Sigma_{nm}^{\text{loc}}$  have to be invariant under all symmetry transformations which belong to the point-group of the lattice. In particular, in a cubic environment (such as a fcc lattice)

$$G_{nm}^{\text{loc}}(\omega) = \hat{G}^{\text{loc}}(\omega) \delta_{nm}, \quad \Sigma_{nm}(\omega) = \hat{\Sigma}(\omega) \delta_{nm}, \quad (2)$$

where  $\hat{G}^{\text{loc}}(\omega)$  and  $\hat{\Sigma}(\omega)$  are scalars. On the surface or in a monolayer the symmetry is lower than cubic and the Green's function has additional off-diagonal parts. However, the corresponding corrections were found to be small (1 % or less) and therefore it is an excellent approximation to use the Green's function and self-energy as given in (2). This yields the scalar equation

$$\hat{\Sigma}(E) = i \sum_{\nu} g_{\nu}^2 \int \frac{d\omega}{2\pi} D_{\nu}^0(\omega) \hat{G}^{\text{loc}}(E - \omega). \quad (3)$$

Thus, the problem is simplified to a single band interacting with a discrete set of phonon modes. Relation (3), which is an equation for the self-energy, is solved iteratively using the advanced Green's function. In (3), the band-structure only enters via the density of states (DOS) and we chose a generic square DOS with a width  $W = 0.5$  eV. Using other bare DOS revealed that the interacting DOS depends only weakly on the form of the bare DOS. The result for half-filling ( $\mu = 0$ ), which corresponds to  $\text{K}_3\text{C}_{60}$ , is shown in Fig. 1. The interacting DOS shows an overall structure, such as a dip at 0.2 eV and a second hump at 0.4 eV, which agrees well with the AIPES of the monolayer system [4].

The insulating compounds  $\text{K}_4\text{C}_{60}$  and  $\text{K}_6\text{C}_{60}$  differ importantly from  $\text{K}_3\text{C}_{60}$ . As discussed in the introduction, in the absence of metallic screening, the coupling to the  $\text{K}^+$  modes is strong and the ground state of a hole created by photoemission will be polaronic. This type of physics is not captured by NCA. On the other hand, the ground states of the insulating phases are rather simple:  $\text{K}_6\text{C}_{60}$  is a trivial band insulator, whereas in  $\text{K}_4\text{C}_{60}$  there are four localized electrons on each  $\text{C}_{60}$  which form a singlet due to Jahn-Teller distortions [13, 19]. If the ground state  $|\Psi_0\rangle$  is known, the moments  $\mu_k = \int d\epsilon \epsilon^k P(\epsilon)$  of

Mode	$\omega_{\nu}$	$\lambda_{\nu}/N(0)$	$g_{\nu}$
$H_g(8)$	195	23	82
$H_g(7)$	177	17	67
$H_g(6)$	155	5	34
$H_g(5)$	136	12	50
$H_g(4)$	96	18	51
$H_g(3)$	88	13	41
$H_g(2)$	54	40	57
$H_g(1)$	34	19	31
$A_g(2)$	182	11	55
$A_g(1)$	61	0	0
K-mode	8.9 <sup>a</sup> , 10.9 <sup>b</sup>	-	65 <sup>a</sup> , 72 <sup>b</sup>
Acoustic	3.8	-	10

TABLE I: Frequencies and coupling constants for the vibrational modes in  $\text{K}_n\text{C}_{60}$  (all energies are in meV). Parameters for the intramolecular  $H_g$  and  $A_g$  modes were taken from Ref. 12. The coupling constant for the lattice vibrations were calculated in this work. In  $\text{K}_3\text{C}_{60}$  the coupling to the  $A_g$  modes and the vibrations of the ionic lattice is efficiently suppressed by metallic screening. a) applies for  $\text{K}_4\text{C}_{60}$ . b) applies for  $\text{K}_6\text{C}_{60}$ .

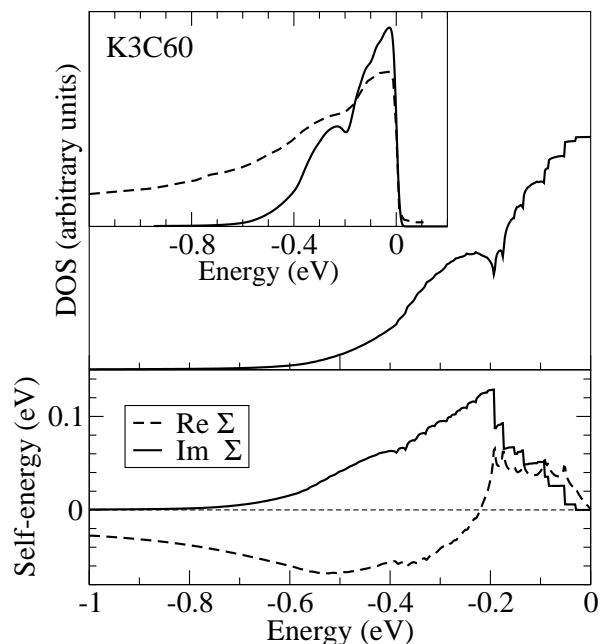


FIG. 1: Solution of the NCA at half filling ( $\mu = 0$ ) which corresponds to  $\text{K}_3\text{C}_{60}$ . *Upper panel:* Occupied part of the interacting DOS. *Lower panel:* Advanced self-energy. *Inset:* Occupied DOS (solid line) convoluted with a Gaussian ( $\sigma = 10$  meV) and compared to the experimental spectrum of the monolayer (dashed line) [4].

the spectrum  $P(\epsilon)$  (normalized to 1) can exactly be calculated by evaluating the expectation values

$$\mu_k = \frac{1}{N} \sum_{jn} \langle \Psi_0 | c_{jn}^\dagger [c_{jn}, \underbrace{H}_{k} \dots] | \Psi_0 \rangle. \quad (4)$$

The sum is over all sites  $j$  and orbitals  $n$  and  $N$  is the total number of the electrons.  $H$  is the full Hamiltonian and includes all vibrational modes as well as Coulomb in-

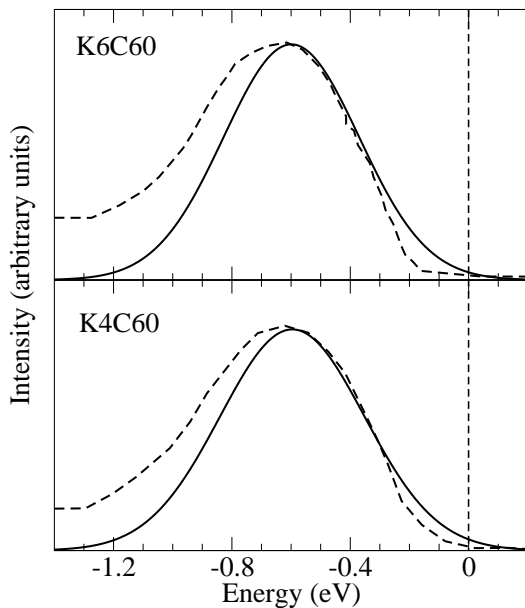


FIG. 2: Gaussian fit (solid curves) to the photoemission spectrum using the first and second moment as calculated in (4) and plotted with respect to the chemical potential. The dashed curves are the experimental data (Ref. 2 for  $K_6C_{60}$ , Ref. 3 for  $K_4C_{60}$ )

interactions. Although relation (4) is exact, the reconstruction of a distribution from a finite number of known moments is an ill-defined problem if the overall shape of the distribution is unknown. However, as was argued above, the strong coupling to the low-energy optic modes yields a very incoherent, and therefore Gaussian-like spectrum. Hence, for this physical reason the distribution should be well approximated by a Gaussian which is determined by the first and second moment as given by (4). The procedure which follows is, first, to determine all contributions to  $H$  and, second, calculate the moments by (4).

The additional phonon contributions to  $H$  are modes which cause a net shift of the molecular orbitals and therefore are no longer screened in the insulating phases [5, 6]. These modes are the intramolecular  $A_g$  modes and the vibrations of the ionic lattice. In principle, lattice vibrations also couple via a change in hopping, but the corresponding coupling is much smaller [7]. In the case of the two intramolecular  $A_g$ , the frequencies  $\omega_\nu$  and coupling parameters  $g_\nu$  are dispersionless. As for the  $H_g$  modes, the latter is given by  $g_\nu^2 = \frac{3}{2}\omega_\nu\lambda_\nu/N(0)$  (see above) and values were taken from Ref. 12. The coupling to the ionic lattice has been studied much less extensively, mainly because it is negligible in the superconducting  $K_3C_{60}$ . Here we consider the coupling due to the Coulomb interaction between the ionic charges. The mass ratio  $M_{C_{60}}/M_K = 18.4$  is big which allows to separate the lattice vibrations into optic dispersionless  $K$ -modes and acoustic modes. The frequencies of these modes were measured by EELS [14] where it was

observed that  $K^+$  ions close to the surface have substantially lower frequencies. As photoemission is surface sensitive, we use these values which are  $\omega_K = 8.9$  meV and  $\omega_K = 10.9$  meV for  $K_4C_{60}$  and  $K_6C_{60}$  respectively. In what follows, only the averaged coupling constant  $\bar{g}_K^2 = N_s^{-1} \sum_{\mathbf{q}\alpha} |g_{\mathbf{q}\alpha}|^2$  enters (the sum is over all optic  $K$ -modes  $\alpha$ ) which is given by (with  $\hbar$  exceptionally included)

$$\bar{g}_K^2 = \frac{e^2\hbar}{2M_K\omega_K} \sum_{r \in \{K^+\}} \mathbf{E}_r^2. \quad (5)$$

The sum runs over all  $K^+$  ions  $r$  and  $\mathbf{E}_r$  is the electric field at the positions  $r$  and caused by an additional hole on the  $C_{60}$  molecule at the origin. The sum in (5) depends on the lattice.  $K_6C_{60}$  has a bcc lattice with a cubic lattice constant  $a = 11.39$  Å where each  $C_{60}$  molecule is surrounded by 24  $K^+$  ions located at  $(0, 0.5, 0.25)a$  [16]. Considering the bare coupling of the closest by  $K^+$  ions yields  $g_K = 120$  meV. Taking into account the polarizability of the  $C_{60}^{6-}$  ions by multipole expansion [17] reduces the electric fields entering (5) by 40 % and yields a coupling constant  $g_K = 72$  meV. In  $K_4C_{60}$  distances between  $C_{60}^{4-}$  and  $K^+$  are almost the same as in  $K_6C_{60}$ , however, every  $C_{60}^{4-}$  ion is surrounded by 16  $K^+$  ions instead of 24. This reduces  $g_K$  in  $K_4C_{60}$  by a factor  $\sqrt{2/3}$  with respect to  $K_6C_{60}$ . Taking also into account the difference in  $\omega_K$  we find  $g_K = 65$  meV for  $K_4C_{60}$ . Coupling to the acoustic modes is more involved because both  $\omega_{\mathbf{q}\alpha}$  and  $g_{\mathbf{q}\alpha}$  are  $\mathbf{q}$  dependent. We used a simple spring model parametrized by a phonon frequency of 5 meV at the Brillouin zone boundary [18]. This yields an averaged coupling constant  $\bar{g}_a = 10$  meV. In addition we find an average frequency  $\bar{\omega}_a = N_s^{-1} \sum_{\mathbf{q}\alpha} \omega_{\mathbf{q}\alpha} |g_{\mathbf{q}\alpha}/\bar{g}_a|^2 = 3.8$  meV. Finally, the Coulomb interactions should also be included in  $H$ . However, they vanish in the case of  $K_6C_{60}$  where a single hole is created in a full band. In  $K_4C_{60}$  there is a contribution from the on-site Hund's-rule coupling term which involves an exchange energy  $K = 50$  meV (see Ref. 20 for a detailed description). This term leads to an additional increase of the width of the  $K_4C_{60}$  spectrum.

In the following we will discuss the results for  $K_6C_{60}$  in more detail than those of  $K_4C_{60}$  because the ground state of the latter involves Jahn-Teller distorted molecules and a detailed discussion would go beyond the scope of this letter. As mentioned above, the ground state of  $K_6C_{60}$  is a full band and trivially given by  $|\Psi_0\rangle = \prod_{jn} c_{jn}^\dagger |\text{vac}\rangle$ . Note that  $|\Psi_0\rangle$  doesn't have any phonon excitations. Coulomb terms can be neglected for  $K_6C_{60}$  and the Hamiltonian  $H = H_{\text{kin}} + H_p + H_{ep}$  consists of the kinetic energy, the phonon energies and the electron-phonon coupling terms. As in the previous section we assume a quadratic bare DOS  $\rho_0$  with a width  $W = 0.5$  eV and centered around zero. Using relation (4) to evaluate the moments of the photoemission spectrum one finds that  $\mu_1 = 0$ . The second moment is  $\mu_2 = \mu_2(\rho_0) + \sum_x g_x^2$

where  $\mu_2(\rho_0) = W/(2\sqrt{3})$  is the second moments of the normalized square DOS  $\rho_0$ . The sum is over all phonon modes  $x$ . Similarly, the third moment is  $\mu_3 = -\sum_x w_x g_x$ . Using the parameters as listed in Tab. I one finds  $\sigma = \sqrt{\mu_2} = 0.229$  eV and  $\mu_3/\sigma^3 = -0.319$ . Usually, the photoemission spectrum is plotted with respect to the chemical potential which, per definition, is  $\mu = E_0(N) - E_0(N-1) = -E_0(N-1)$  and therefore corresponds to the polaron ground state energy. In the small polaron limit, where the hole is localized on a single molecule, the chemical potential is given by the relaxation energy of the phonon degrees of freedom which couple to the hole:

$$\mu = -E_0(C_{60}^{1-}) + \frac{\bar{g}_K^2}{\omega_K} + \frac{\bar{g}_a^2}{\bar{\omega}_a} = 0.599 \text{ eV}, \quad (6)$$

$E_0(C_{60}^{1-})$  is the Jahn-Teller ground state energy of an electron in the LUMO of an isolated  $C_{60}$  molecule interacting with the intramolecular modes. By particle-hole symmetry, this is the same as  $E_0(C_{60}^{5-})$  and was calculated numerically in Ref. 19. The last two terms are the energy gain due to the ionic lattice distortions. It must be noted that the total contribution of the K-modes to the chemical potential is proportional to  $w_K^{-2}$ , because  $g_K^2$  itself is proportional to  $w_K^{-1}$  (relation (5)). Hence,  $\mu$  depends sensitively on  $\omega_K$ . Note that this estimate is a lower bound for the chemical potential, because in the insulating  $K_6C_{60}$  it may lay everywhere in the bandgap rather than on the top of the filled band. In Fig. 2 a Gaussian of width  $\sigma$  and shifted by  $\mu$  is plotted. The result compares well with the experimental curve from bulk measurements although the width is somewhat too small [2]. Other fitting functions which accounted correctly for the non-zero third moment were tested as well which, however, yielded only slightly different curves than the Gaussian shown here.

The case of  $K_4C_{60}$  is more complicated, due to Jahn-Teller distorted molecules where the three-fold degenerate LUMO is split into a singlet and a doublet. In  $K_4C_{60}$  the doublet is lower in energy and occupied by four electrons. Hence, they form a full band in the solid which results in the insulating state. The problem of the Jahn-Teller distortion in  $C_{60}$ , which cannot be solved analytically, has been extensively studied by various approaches [13, 19]. In addition, we developed a variational wavefunction for  $C_{60}^{4-}$  which yields a ground state energy in agreement with exact diagonalization results [19]. In order to calculate the expectation values in (4) we use this variational ground state (details of the calculation of the will be published elsewhere). We find a first moment  $\mu_1 = -0.174$  eV which is due to the energy gain of the Jahn-Teller distortion. The chemical potential is again

given by (6), except that  $-E_0(C_{60}^{1-})$  has to be replaced by  $E_0(C_{60}^{4-}) - E_0(C_{60}^{3-})$  which yields  $\mu = 0.422$  eV [19]. Finally, the second moment is  $\sigma = \sqrt{\mu_2} = 0.244$  eV which is almost the same as in  $K_6C_{60}$ . In Fig. 2 the corresponding Gaussian is plotted and compared to the experimental data from bulk measurements [3]. Again, good agreement is found.

In conclusion, we showed that the different photoemission spectra in metallic and insulating  $K_nC_{60}$  are due to a large change in the coupling strength to the low-energy, optic  $K^+$  modes. Theoretical calculations for both cases yield good results.

We are grateful to E. Koch and O. Gunnarsson for useful discussions and, especially, to Z.-X. Shen for drawing our attention to this problem as well as to W.L. Yang for providing the experimental data. We also acknowledge the support from the Swiss Nationalfonds.

---

\* Electronic address: swehrli@phys.ethz.ch

- [1] C.T.Chen et al., Nature **352**, (1991) 603.
- [2] P.J. Benning, Phys. Rev. B **47**, (1993) 13843.
- [3] R. Hesper, L.H. Tjeng, A. Heeres, G.A. Swatzky, Phys. Rev. B **62**, (2000) 16046.
- [4] W.L. Yang et al., Science **300**, (2003) 303; W.L. Yang, Z.-X. Shen, private communication.
- [5] O. Gunnarsson, G. Zwignagel, Phys. Rev. Lett. **69**, (1992) 957; O. Gunnarsson, D. Rainer, G. Zwignagel, Int. J. of Mod. Phys. B **6**, (1992) 3993.
- [6] E. Koch, O. Gunnarsson, R.M. Martin, Phys. Rev. Lett. **83**, (1999) 620.
- [7] O. Gunnarsson, Rev. Mod. Phys. **69**, (1997) 575.
- [8] S. Engelsberg, J.R. Schrieffer, Phys. Rev. **131**, (1963) 993.
- [9] R. Hesper, L.H. Tjeng, G.A. Sawatzky, Europhys. Lett. **40**, (1997) 177.
- [10] A.I. Liechtenstein, O. Gunnarsson, M. Knupfer, J. Fink, J.F. Armbruster, J. Phys. C **8**, (1996) 4001.
- [11] M. Lannoo, G.A. Baraff, M. Schlüter, D. Tomanek, Phys. Rev. B **44**, (1991) 12106.
- [12] O. Gunnarsson et al., Phys. Rev. Lett. **74**, (1995) 1875.
- [13] A. Auerbach, N. Manini, E. Tosatti, Phys. Rev. B **49**, (1994) 12998; Phys. Rev. B **49**, (1994) 13008.
- [14] C. Silien, P.A. Thiry, Y. Caudano, Phys. Rev. B **67**, (2003) 075412.
- [15] A. Cheng, M.L. Klein, J. Phys. Chem. **93**, (1991) 9622.
- [16] S.C. Erwin, M.R. Pederson, Phys. Rev. Lett. **67**, (1991) 1610.
- [17] S. Wehrli, E. Koch, M. Sigrist, Phys. Rev. B **68**, (2003) 115412.
- [18] L. Pintschovius Rep. Prog. Phys. **59**, (1996) 473.
- [19] O. Gunnarsson, Phys. Rev. B **51**, (1995) 3493.
- [20] M. Capone, M. Fabrizio, P. Giannozzi, E. Tosatti, Phys. Rev. B **62**, (2000) 7619.